TITLE: Left ventricle hypertrabeculation/non-compaction and inherited gastropathy associated to *MIB2* variants altering NOTCH signaling.

AUTHORS: Pasquale Piccolo,[1] Sergio Attanasio,[1] Ilaria Secco,[2] Riccardo Sangermano,[1] Caterina Strisciuglio,[3] Giuseppe Limongelli,[4] Erasmo Miele,[3] Margherita Mutarelli,[1] Sandro Banfi,[1] Vincenzo Nigro,[1] Tirso Pons,[5] Alfonso Valencia,[5] Lorena Zentilin,[2] Severo Campione,[6] Gerardo Nardone,[7] Ty C. Lynnes,[8] Patricia B.S. Celestino-Soper,[8] Katherine G. Spoonamore,[8] Franco D'Armiento,[6] Mauro Giacca,[2,10] Annamaria Staiano,[3] Matteo Vatta,[8,9] Chiara Collesi,[2,10] and Nicola Brunetti-Pierri[1,3]

INSTITUTIONS: [1]Telethon Institute of Genetics and Medicine (TIGEM), Pozzuoli, Napoli, 80078 Italy; [2]Molecular Medicine Laboratory, International Centre for Genetic Engineering and Biotechnology, Trieste, 34149 Italy; [3]Department of Translational Medicine, Federico II University, Naples, 80131 Italy; [4]Monaldi Hospital, Second University of Naples, Naples, 80131 Italy; [5]Structural Biology and BioComputing Programme, Spanish National Cancer Research Centre (CNIO), Madrid, E-28029 Spain; [6]Advanced Biomedical Sciences, Federico II University, Naples, 80131 Italy; [7]Department of Clinical Medicine and Surgery, Gastroenterology Unit, Federico II University, Naples, 80131 Italy; [8]Department of Medical and Molecular Genetics and the [9]Krannert Institute of Cardiology, Division of Cardiology, Department of Medicine, Indiana University School of Medicine, Indianapolis, IN, 46202 USA; [10]Department of Medical, Surgical and Health Sciences, University of Trieste, Trieste, Italy.

CORRESPONDING AUTHOR: Nicola Brunetti-Pierri, MD

Telethon Institute of Genetics and Medicine

Via Campi Flegrei 34

80078, Pozzuoli (NA), ITALY

This is the author's manuscript of the article published in final edited form as:
Piccolo, P., Attanasio, S., Secco, I., Sangermano, R., Strisciuglio, C., Limongelli, G., ... & Pons, T. (2017). MIB2 variants altering NOTCH signalling result in left ventricle hypertrabeculation/non-compaction and are associated with Ménétrier-like gastropathy. Human molecular genetics, 26(1), 33-43. https://doi.org/10.1093/hmg/ddw365

Phone: +39 081 6132361

Fax: +39 081 5609877

E-mail: brunetti@tigem.it

ABSTRACT

We performed exome sequencing in patients from a family of Italian descent with an autosomal dominant gastropathy resembling Ménétrier disease, a premalignant disorder of the stomach with epithelial hyperplasia and enhanced EGFR signaling due to local overproduction of TGF-α. Ménétrier disease is believed to be an acquired disorder but its etiology is unknown. In affected patients, we found a missense p.V742G variant in *MIB2*, a gene regulating NOTCH signaling that has not been previously linked to human diseases. The variant segregated with the disease in the pedigree, affects a highly conserved amino acid residue, and was predicted to be deleterious although it was found with a low frequency in control populations. The purified protein carrying the p.V742G variant showed reduced ubiquitination activity in vitro and white blood cells from patients exhibited significant reductions of *HES1* and *NOTCH3* expression reflecting alteration of NOTCH signaling. Because mutations of MIB1, the homolog of MIB2, have been found in patients with left ventricle non-compaction (LVNC), we screened members of the family with Ménétrier-like disease for this cardiac abnormality. Asymptomatic left ventricular hypertrabeculation, which is the mildest end of the LVNC spectrum, was detected in two members carrying the *MIB2* variant. Finally, we identified a *MIB2* variant (p.V984L) affecting protein stability in an unrelated patient with LVNC. Expression of both MIB2 variants affected NOTCH1 signaling, proliferation and apoptosis in primary cardiomyocytes.

In conclusion, we report the first example of left ventricular hypertrabeculation/LVNC with germline *MIB2* variants resulting in altered NOTCH signaling that might be associated with a gastropathy clinically overlapping with Ménétrier disease.

TEXT

Whole exome sequencing (WES) is a powerful tool in identifying disease-associated variants in a wide variety of genetic diseases[1]. In this study, we performed WES on a family of Italian descent with multiple members presenting with an autosomal dominant gastropathy with Ménétrier-like features[2] (**Fig. 1A**). Ménétrier disease is a premalignant disorder of the stomach presenting with gross cerebriform hypertrophy of gastric mucosa confined to the body and fundus with sparing of the antrum[3; 4]. Enhanced epidermal growth factor receptor (EGFR) signaling due to local overproduction of transforming growth factor-α (TGF-α) that results in expansion of surface mucous cells in the body and fundus of the stomach[5-8] has been shown in affected patients[3]. Therefore, patients with Ménétrier disease are treated with Cetuximab, a monoclonal antibody blocking EGFR signaling[9]. Nevertheless, the underlying molecular defect(s) that results in upregulation of TGF-α in Ménétrier disease is still unknown and TGF-α is not overexpressed elsewhere in the body of individuals with Ménétrier disease[3]. Familial occurrence of Ménétrier disease has been rarely reported[10,4,11]. Unraveling the molecular defects underlying rare familial forms might provide hints to understand the molecular basis of Ménétrier disease. Like classic Ménétrier syndrome, the gastric lesions in the family with Ménétrier-like syndrome[2] showed EGFR overexpression (**Fig. 1B**). WES was performed on four affected members of the family (subjects II.2, II.4, IV.2, and IV.5 of **Fig. 1A**). Given the autosomal dominant pattern of inheritance, we focused on single nucleotide variations and small insertions and deletions (indels) in heterozygous state. We selected only heterozygous variants falling within coding regions not predicted to generate synonymous amino acid changes, affecting all four samples analyzed, and presenting with sufficient depth and quality. Eight single nucleotide substitutions passed this filtering process (**Table 1**). Among these, six were described in ExAC database with frequency >0.01 and were discarded. The two remaining variants in nucleoporin-98 (*NUP98*) and mind-bomb 2 (*MIB2*) were confirmed by Sanger sequencing and analyzed for phenotype segregation among affected family members. We observed segregation in all ten affected members with available DNA only for the

c.2225T>G (p.V742G) heterozygous variant in *MIB2* gene (**Fig. 1A**). Subject III.3 was asymptomatic and never underwent gastric endoscopy but was an obligate carrier having transmitted the disease to his child. Asymptomatic subject III.4 who did not carry the *MIB2* variant was evaluated by gastric endoscopy that failed to show the abnormalities observed in the other family members. The p.V742G variant was found with a low frequency of 0.00055 in European non-Finnish population and with a cumulative frequency of 0.00147 in control populations (**Table 2**). This variant was detected in the homozygous state in two Asian individuals reported in the ExAc database. Nevertheless, the variant changes a highly conserved valine into glycine at the amino acid position 742 that is predicted to be deleterious by multiple methods (**Supplementary Table 1**). The Val742 is positioned towards C-terminus in a highly conserved ankyrin repeat (a.a. 717-769; Pfam ID: PF13637) suggesting that the p.V742G variant might result in structural and/or functional effects disturbing the hydrophobic packing between α helices which destabilize the helix-turn-helix fold of the ankyrin repeat (**Fig. 2A**)[12; 13]. Clustering of disease-related variants in regions of the three-dimensional structure is sometimes used as supporting evidence for the pathogenicity[14] and known cancer-related variants, such as p. A752V (Liver) and p. D775N (Lung), are also positioned in this ankyrin repeat, and nearby p.V742G, according to Structure-PPi method[15]. Another single nucleotide variant in *MIB2* gene, c.214T>C (p.F72L) was found either in homozygous or heterozygous states in all affected family members (**Supplementary Fig. 1**) and this variant has a cumulative frequency of 0.6228 in controls (**Table 2**). Among the other variants detected by the exome, we also found the c.98C>G (p.P33R) variant in *TP53* gene that has been reported among the polymorphisms associated with the risk of cancer of the stomach[16] and gastrointestinal tract[17].

Because *MIB1* mutations were recently found to be responsible for left ventricle non-compaction (LVNC)[18], we evaluated 4 family members for this heart defect by cardiac ultrasound, even though none of them had cardiac complaints. The cardiac ultrasound followed by cardiac MRI revealed in two (III.6 and IV.2) of four (III.2, III.6, IV.2, IV.5) family members carrying the *MIB2*

variant enhanced apical trabeculation of the left ventricle which is consistent with an incomplete phenotype of LVNC (**Fig. 1A, C**).

We next evaluated a small group of patients with cardiomyopathy and left ventricular hypertrabeculation or isolated LNVC who previously underwent extensive clinical testing for a panel of 38 cardiomyopathy genes (see Methods) by next generation sequencing (n=7). We identified a c.2950G>C (p.V984L) variant in *MIB2* gene in a 47 year-old African American woman with typical LVNC who presented with symptoms of paresthesia and chest pain. Echocardiogram revealed an ejection fraction (EF) of 48% and mild left atrium (LA) and right atrium (RA) dilation along with hypertrabeculated left ventricle (LV) consistent with the diagnosis of LVNC (**Fig. 1C**). The cardiac MRI identified increased left ventricular trabeculation with deep intratrabecular recesses of the apex extending to the mid LV, with a noncompacted to compacted myocardium ratio at the LV apex of 5:1, thus confirming the diagnosis of LVNC (**Fig. 1C**). In addition, the systolic function was found to be only mildly reduced with an EF of 46%, while the LA and RA appeared normal in size. There were no apparent valve abnormalities and there was no delayed gadolinium enhancement. The electrocardiogram (ECG) showed sinus rhythm with premature supraventricular complexes, nonspecific T wave abnormality with a QTc interval of 450 ms (**Supplementary Fig. 2**). The patient did not have gastrointestinal complaints. She belongs to a family with several siblings and she is the only member who currently has a diagnosis of LVNC. Both maternal and paternal ancestry is African American. However, consanguinity was denied. The family history was negative for diagnoses of hypertrophic cardiomyopathy (HCM) and/or non-ischemic dilated cardiomyopathy (DCM), sudden death or implantable cardioverter defibrillator (ICD) placement, although both parents suffered a myocardial infarction consistent with coronary artery disease and some of her siblings had unspecified cardiac symptoms. Echocardiogram in the mother did not identify any major left ventricular abnormalities. Both parents and other family members were unavailable for genetic testing, thus segregation analysis was not possible.

The p.V984L variant is not present in EVS while it is reported in ExAC in 1 out 102,118 alleles ($9.8x10^{-6}$) (**Table 2**). The variant changes a valine into leucine at the conserved amino acid position 984 but is not predicted to be deleterious by prediction methods (**Supplementary Table 1**). Nevertheless, the variant is predicted to affect the 3D stability of the protein (**Supplementary Table 1**). The Val984 is located in the linker region between two zinc-fingers RING type motifs (a.a. 945-987; Pfam ID: PF13920), and in the vicinity of the ligand-binding cysteine residues and also the cancer variant p.I979M (**Fig. 2B**). Moreover, Val984 is conserved in homolog MIB1 protein and the same region of MIB1 protein was previously found to be affected by a mutation responsible for LVNC[18].

To investigate whether the *MIB2* variants result in impaired protein function, we performed an *in vitro* functional ubiquitination assay (**Fig. 2C** and **D**). MIB2 protein was previously shown to undergo auto-ubiquitination[19]. Purified recombinant $MIB2^{WT}$, $MIB2^{V742G}$ and $MIB2^{V984L}$ proteins were incubated with E1, E2 proteins, and FLAG-ubiquitin to measure auto-ubiquitination activity by Western blotting. The protein band detected by the antibody against the ubiquitin-FLAG was reduced in the $MIB2^{V742G}$ mutant compared to the wild-type protein. Therefore, $MIB2^{V742G}$ is less auto-ubiquitinated compared to the wild-type protein, suggesting a reduced ubiquitin ligase activity. In contrast, the $MIB2^{V984L}$ mutant was not found to affect its auto-ubiquitination activity (**Fig. 2C, D**). Nevertheless, the levels of this mutant protein were significantly reduced by Western blotting performed with two different antibodies recognizing different protein epitopes in transfected HeLa cells (**Supplementary Fig. 3**), even though no significant differences were observed in the mRNA levels of *MIB2* and GFP protein levels used as an internal control of transfection efficiency (**Supplementary Fig. 3**). To investigate the degradation rate of MIB2 mutants, HEK293 cells were first transfected with Flag-tagged $MIB2^{WT}$, $MIB2^{V742G}$ or $MIB2^{V984L}$ and then treated with cycloheximide (CHX) to block protein synthesis; MG132 was used as control to inhibit proteasomal degradation of transfected proteins. Western blot analysis for MIB2 showed significantly reduced degradation rate for $MIB2^{V742G}$ compared to the wild-type protein while the $MIB2^{V984L}$ protein

could only be detected after MG132 treatment, suggesting rapid proteasomal degradation (**Fig. 2E-F**). Transgene expression was confirmed by real time PCR that did not show differences among transfected plasmids **(Supplementary Fig. 4**).

Previous studies have shown that both MIB1 and MIB2 regulate NOTCH activity[20; 21]. Therefore, we evaluated NOTCH signaling genes in RNA extracted from white blood cells of two affected members from pedigree 1 (III.6 and IV.5) that were compared to age- and gender-matched controls. Significant reductions of *HES1* and *NOTCH3* expression were detected in both patients while *NRARP* expression was significantly down-regulated in patient III.6 compared to corresponding controls and showed a trend in reduction in patient IV.5 (**Fig. 3**). Taken together, these data show decreased NOTCH signaling in white blood cells carrying the p.V742G variant. Blood sample for RNA analysis was not available for the isolated case of LVNC carrying the p.V984L variant.

To investigate the consequence of MIB2 variants on NOTCH signaling, neonatal rat cardiomyocytes were infected with adeno-associated viral vectors (AAV6) expressing $MIB2^{V742G}$, $MIB2^{V984L}$ or $MIB2^{WT}$ and were also transfected with a plasmid bearing the luciferase gene under the control of an artificial NOTCH1 responsive element containing four repeats of the CBF1 binding sites[22]. AAV6 vectors have shown robust and persistent transgene expression in cardiomyocytes[23]. To distinguish specific NOTCH-mediated transactivation effect triggered by the transgenes delivered by the AAV6, cardiomyocytes were grown in the presence of a γ-secretase inhibitor [DAPT (N-[N-(3,5-difluorophenacetyl)-L-alanyl]-S-phenylglycine t-butyl ester)] to inhibit endogenous NOTCH1 receptor signaling[24]. Transcriptional activation of NOTCH regulatory elements by either $MIB2^{V742G}$ or $MIB2^{V984L}$ was reduced compared to $MIB2^{WT}$ (**Fig. 4A**). Cardiomyocytes transduced with the vector encoding $MIB2^{V742G}$ also showed decreased vitality compared to $MIB2^{WT}$ control; only a trend in reduction of vitality was observed in cells transduced with the $MIB2^{V984L}$ (**Fig. 4B**). To determine whether MIB2 mutants affect cardiomyocyte proliferation, incorporation of thymidine analogue 5-ethynyl-2'-deoxyuridine (EdU) was evaluated

in cardiomyocytes transduced with AAV6 encoding wild-type or MIB2 variants. $MIB2^{WT}$ increased the number EdU-positive and α-actinin-positive cells whereas $MIB2^{V742G}$ variant decreased the number of proliferating rat cardiomyocytes (**Fig. 4C-D**). A trend in reduction of proliferating cells was detected in cells transduced with $MIB2^{V984L}$ (**Fig. 4C-D**).

We report herein the first example of inherited disorder with left ventricular hypertrabeculation/LVNC due to *MIB2* mutations altering NOTCH signaling. Patients of a large pedigree analyzed herein harboring the p.V742G variant in *MIB2* gene also showed clinical features of a gastropathy that closely resembles Ménétrier disease[2]. Within the affected family members with Ménétrier-like disease, at least one individual (III.3) carrying the p.V742G variant was free of gastric symptoms suggesting incomplete penetrance of the stomach disease. Variable expressivity of the gastric phenotype was also observed[2]. Nevertheless, the low frequency of the p.V742G variant in the control population and the rare occurrence of Ménétrier-like syndrome suggest that the *MIB2* variant is not the only cause for the gastropathy. In addition to *MIB2* mutations, other genes or environmental factors could be necessary for clinical expression of the gastropathy. The affected family members were also found to harbor the polymorphisms p.F72L in *MIB2* gene p.P33R in *TP53* gene. We speculate that the inheritance of the combination of either or both polymorphisms with the p.V742G variant might play a role in the expression and severity of the gastric phenotype.

Ménétrier disease has been previously linked to infection with CMV, particularly in children[25], and *Helicobacter pylori*[3]. Interestingly, both CMV and *Helicobacter pylori* have been found to downregulate NOTCH expression[26 27]. However, it should be noted that no evidence of infections by CMV and *Helicobacter pylori* was detected in the index cases of the pedigree[2]. Nevertheless, additional yet unidentified genetic, epigenetic[28] or environmental factor(s) might affect NOTCH signaling thus resulting in the expression of the disease.

NOTCH signaling is critical for cell-fate determination and is involved in maintaining the balance between cell proliferation and differentiation[29]. The gastric epithelium is continuously

regenerated by gastric stem cells that give rise to various cell types including parietal cells, chief cells, surface mucous cells, mucous neck cells, and enteroendocrine cells. The region in which progenitor cells are found is located at the isthmus of the gastric glands. From this region, precursor cells give rise to surface mucous cells that move to the luminal surface of the glands, parietal cells that move to the base of the glands, and mucous neck cells which also migrate down and further differentiate into chief cells. NOTCH signaling is required to maintain the gastric stem cell compartment[30]. Therefore, it is not surprising that alteration of NOTCH signaling in the stomach might lead to gastric hypertrophy. Cross-talk between EGFR and NOTCH has been previously reported[31] and could be responsible for the increased EGFR expression observed in the patients. Although some differences exist between Ménétrier-like observed in the family and classic Ménétrier disease[2], we speculate that NOTCH pathway might also be involved in the pathogenesis of Ménétrier syndrome.

Several genes have been linked to LVNC and they encode proteins involved in cellular energy, muscle development, ion channel formation, or components of the muscle filaments[32-34]. Altogether, these defects show that LVNC is caused by at least two final common pathways: a primary pathway (such as the sarcomere) and a developmental pathway (such as the NOTCH pathway)[35; 36]. Evidence from mouse developmental studies show that hypertrabeculation results from altered regulation of cell proliferation, differentiation, and maturation during the formation of the ventricular wall, particularly if the NOTCH signaling pathway is affected[37]. Inactivation of NOTCH pathway genes such as *Notch1*, *Rbpj*, or *Fkbp1a* in mice results in disruption of trabeculation of ventricular chamber and spongy myocardial wall[38,39; 40]. Further support for the role of NOTCH pathway in LVNC was confirmed in humans with autosomal dominant LVNC and germline mutations in *MIB1* gene[18]. Similarly to *MIB2* variants reported herein, two *MIB1* mutations previously found in patients with LVNC also affect the ankyrin repeat and the zinc-finger RING type motif[18], thus suggesting the important roles of these domains in protein function or stability.

The diagnosis of LVNC relies on non-invasive imaging studies, usually echocardiography and cardiac MRI. However, the diagnostic criteria for both these methods are still debated and are currently based on measurements of the ratio of the thickness of the non-compacted layer to that of the compacted layer[41]. Such criteria were present in two patients with left ventricular hypertrabeculation/LVNC carrying the p.V742G variant in *MIB2* gene. Healthy individuals and competitive athletes may fulfill current imaging criteria for diagnosis of LVNC presenting with normal left ventricular size and preserved systolic and diastolic functions. This has been considered a benign variant[39; 42]. Therefore, it has been proposed that the extent of myocardial compaction may be a continuous spectrum within the population ranging from asymptomatic individuals to end stage heart failure. Based on the lack of cardiac complains and altered heart function in the patients with p.V742G variant and the very low frequency of *MIB2* variant in the population, we argue that at least a subgroup of individuals with benign LVNC might harbor *MIB2* mutations. It remains to be ascertained whether and which additional hits, either genetic or environmental, are needed for the development of overt cardiac disease. The identification of a larger number of individuals harboring *MIB2* mutations will allow understanding the full spectrum of cardiac and gastric phenotype associated with mutations in this gene.

In conclusion, we found that germline *MIB2* variants resulting in altered NOTCH signaling are associated with a spectrum of left ventricular hypertrabeculation/LVNC and might be associated with hypertrophic gastropathy clinically overlapping with Ménétrier disease.

PATIENTS AND METHODS

Patients

The clinical findings of the family with inherited gastropathy and LVNC (**Fig. 1A**) are described in greater details elsewhere[2]. The patient with LVNC (**Fig. 1B**) was part of a highly selected case series of patients with cardiomyopathy and left ventricular hypertrabeculation or isolated LVNC. This patient underwent clinical genetic testing for a next generation sequencing

panel of 38 genes associated with various forms of cardiomyopathies including *ACTC1, ACTN2, ANKRD1, CSRP3, DES, EMD, LAMP2, LMNA, MTND1, MTND5, MTND6, MTTD, MTTH, MTTI, MTTK, MTTL1, MTTL2, MTTM, MTTQ, MTTS1, MTTS2, MYBPC3, MYH7, NEXN, PLN, RBM20, SCN5A, SGCD, TAZ, TCAP, TNNC1, TNNI3, TNNT2, TPMI, TTN, TTR, VCL, ZASP*.

Exome sequencing

Exome sequencing was performed on DNA samples extracted from peripheral blood of four patients in two different sessions. Samples from patients IV.2 e IV.5 were performed by hybridization of shotgun fragment libraries to the Agilent SureSelect Human All Exon v1 (Agilent Technologies, Santa Clara, CA, USA) in-solution capture assays and libraries were sequenced using the SOLiD system v3.5 (Life Technologies, Carlsbad, CA, USA) according manufacturer's instructions. The sequences were analyzed using an automated custom pipeline. Sequencing reads were first colour-corrected using SOLiD Accuracy Enhancer Tool (SAET), then mapped to the reference genome (UCSC, hg19 build) using the software BioScope v1.3 (Life Technologies) and duplicate reads were removed using Picard (http://picard.sourceforge.net). Single nucleotide variations (SNV) and in-del mutation calling analyses were carried out using the appropriate BioScope calling module: diBayes algorithm with medium stringency settings and the SOLiD Small Indel Fragment Tool, respectively.

Samples from patients II.2 e II.4 were performed by hybridization of shotgun fragment libraries to the Illumina TruSeq Exome Enrichment Kit (Illumina inc., San Diego, CA, USA) and libraries were sequenced using the HiSeq1000 system (Illumina) according manufacturer's instructions. The sequences were analyzed using an automated custom pipeline also available as web resource[43]. Paired sequencing reads were aligned to the reference genome (UCSC, hg19 build) using BWA [44] and post-alignment process and duplicate removal was performed using SAMtools [45] and Picard. Further processing (local realignment around in-del and base recalibration) and SNV and in-del calling were performed with Genome Analysis Toolkit (GATK)[46].

The called SNV and indel variants produced with both platforms were annotated using ANNOVAR [47] with: the relative position in genes using the RefSeq [48] gene model, amino acid change, presence in dbSNP (v137) [49] and in known disease-associated databases [50-52], frequency in Exome Aggregation Consortium (ExAC) (v0.3), NHLBI Exome Variant Server, 1,000 genomes project [53], multiple cross-species conservation [54; 55] and prediction scores of damaging on protein activity [56-60].

The annotated results were then imported into an in-house variation database, also used to make comparisons among samples and filter results. The alignments at candidate positions were visually inspected using the Integrative Genomics Viewer (IGV) [61]. MIB2 mutations were confirmed by Sanger sequencing (Primm, Milan, IT).

Computational analysis

Prediction of deleterious effect of the identified variants was performed by a combined approach using: 1) prediction of variant pathogenicity; 2) prediction of protein stability changes; and 3) functional annotations that overlap or are in close proximity to the affected residues. Human MIB2 (UniProt accession: Q96AX9) is a multi-domain protein with 1070 amino acids whose three-dimensional (3D) structure has not been determined yet. *MIB2* gene codes for 17 protein-coding transcripts, according to Ensembl database (http://www.ensembl.org/), therefore in the present manuscript the nucleotide and amino acids sequences are numbered according to RefSeq ID (NM_080875) and Ensembl protein ID (ENSP00000426103), respectively. Notice that the Ensembl protein sequence (ENSP00000426103) differs from the UniProt reference sequence (Q96AX9). Only a few 3D models of the human MIB2 are available at ModBase (https://modbase.compbio.ucsf.edu/), a repository that collects comparative protein structure models. The sequence identity between MIB2 (a.a. 658-772) and a designed ankyrin repeat protein whose crystal structure was used as template (PDB ID: 1n0r, chain A, 1.5Å resolution), is 46%, well above the threshold of 30% for reliable fold assignment. We next focused on the 3D modeling

of the MIB2 region 945-987, which accommodates the missense variant p.V984L and a Zinc-finger RING type motif. We submitted the MIB2 sequence to the I-TASSER method (http://zhanglab.ccmb.med.umich.edu/I-TASSER) for 3D modeling. The *ab* initio 3D model calculated by I-TASSER shows a 33% sequence identity with the crystal structure of Baculoviral cIAP2 RING domain (PDB ID: 3eb5, chain A, 2.0Å resolution).

To gain insight into the putative functional effects of the MIB2 variants, we mapped p.V742G and p.V984L onto 3D models. We also used the dbNSFP v2.8 database[62] to obtain the damage prediction of identified missense variants by PolyPhen-2, SIFT, MutationAssessor, SVM, and VEST3. For the identified variants, protein stability calculations were performed using CUPSAT (http://cupsat.tu-bs.de), I-Mutant 2.0 (http://folding.biofold.org/i-mutant/i-mutant2.0.html), and PoPMuSiC (http://dezyme.com). Functional annotations (e.g., ligand-binding residues, protein domains, reported variants in COSMIC database, UniProt annotations for missense variants that overlap the mutation position, residues located in close physical proximity or that affect protein interaction surfaces) were retrieved with the Structure-PPi method available at http://structureppi.bioinfo.cnio.es/Structure[15].

In vitro ubiquitination assay

Full-length human *MIB2* cDNA in pCMV-Sport6 backbone was purchased from Open Biosystems (GE Healthcare, Pittsburgh, PA, USA). The *MIB2* mutant constructs (MIB2_V742G and MIB2_V984L) were generated using QuikChange II XL-site-directed mutagenesis (Agilent Technologies), according to manufacturer's instructions. The cDNAs which encoded full length *MIB2* were subcloned into a pGEX-4T-3 GST expression vector (GE Healthcare). Cloned cDNA full-length sequences were confirming by Sanger sequencing (Primm). GST-tagged *MIB2* constructs were expressed in Rosetta (DE3) cells using isopropyl-1-thio-β-D-galactopyranoside (IPTG) (Sigma-Aldrich). Recombinant proteins were affinity-purified using glutathione Sepharose

4B resin (GE Healthcare). Purified proteins were then analyzed by sodium dodecyl sulfate (SDS)-polyacrylamide gel electrophoresis (PAGE) and Coomassie Brillant Blue.

In vitro ubiquitination assay was performed according to a modified version of methods previously reported[20]. Recombinant ubiquitin-activating enzyme E1 (Sigma-Aldrich, St. Louis, MO, USA) and GST-fused MIB2 proteins were mixed into a reaction mixture containing 50 mmol/L Tris-HCl pH 7.4, 5 mmol/L $MgCl_2$, 4 mmol/L ATP, 0.5 mmol/L dithiothreitol, 15 µg of FLAG-ubiquitin (Sigma-Aldrich), and incubated in equimolar amounts human His-tagged UbcH5b (E2) (BioVision, Milpitas, CA, USA) at 30°C for 4 hours. Proteins were then subjected to SDS PAGE under reducing conditions and detected by western blotting using primary antibodies to the FLAG tag (Sigma-Aldrich) or to MIB2 (Novus Biological, Littleton, CO, USA) protein. ECL anti-mouse and anti-rabbit HRP secondary antibodies (GE Healthcare) were used for FLAG and MIB2, respectively. Analysis of band intensities was performed using Quantity One basic software (Bio-Rad Laboratories, Hercules, CA, USA).

Expression of MIB2 mutants

HeLa cells (ATCC) were co-transfected with pCMV-GFP and plasmid expressing either wild-type, MIB2 mutants, or p3xFLAG-CMV-14 (Sigma-Aldrich) with Lipofectamine2000 (Life Technologies) according to manufacturer's instructions. 18 hours post-transfection, proteins and RNA were extracted in either RIPA buffer or with RNeasy kit (Qiagen). Proteins were analyzed by western blotting using rabbit anti-MIB2 (Novus Biological), mouse anti-MIB2 (Abcam, Cambridge, UK), and anti-GFP (Life Technologies). Anti-GAPDH (Santa Cruz Biotechnology) was used for normalization. ECL anti-rabbit or anti-mouse HRP to MIB2, and ECL anti-mouse HRP to GFP and GAPDH were used as secondary antibodies (GE Healthcare). RNA was reverse transcribed using a first-strand complementary deoxyribonucleic acid kit with random primers according to manufacturer's protocol (Life technologies, Grand Island, NY, USA). The qPCR reactions were performed using Roche Light Cycler 480 system (Roche, Indianapolis, IN, USA). PCR reactions

were performed with SYBR Green Master Mix (Roche). PCR conditions were as follows: pre-heating, 5 minutes at 95°C; 40 cycles of 15 seconds at 95°C, 15 seconds at 60°C, and 25 seconds at 72°C. Quantification results were expressed in terms of cycle threshold (Ct). For the expression analysis GUSB and HPRT1 housekeeping genes were used as endogenous controls (reference markers) using LightCycler 480 software v1.5. Differences between mean C_t values of tested genes and those of the reference gene were calculated as ΔC_t gene = C_t gene - C_t reference. WT1 sample was used as calibrator and relative fold increase in expression levels was determined as $E^{-\Delta\Delta Ct}$, E being primer efficiency. The Ct values were averaged for each technical duplicate. Primers to *MIB2* and *GFP* are reported in **Supplementary Table 2. Analysis of protein stability**

MIB2wt-Flag, MIB2V742G-Flag and MIB2V984L-Flag were transfected in Hek 293 cells using a standard Calcium Phosphate protocol. 24 hrs after transfection, the medium was supplemented with 10 µg/ml cycloheximide (CHX; Calbiochem) for 1, 2, 3 and 4 hrs prior to cell lysis in RIPA Buffer (50 mM Tris-HCl, 150 mM NaCl, 5 mM EDTA, 5 mM EGTA, 0.5% NaDoc, 1% Triton X-100, and 0.1% SDS) supplemented with 90 µg/ml PMSF, 1 mM $NaVO_4$ (all from Sigma) and proteases inhibitors (Roche). The proteasome inhibitor MG132 (Calbiochem) was supplemented at a concentration of 10 µM for 4 hr. After sonication and pre-clearing, protein lysate concentration was determined by Bradford Assay (BIORAD). Equal amounts of protein were resolved on 8% SDS-PAGE mini-gels and transferred to nitrocellulose membranes (GE Healthcare). Western Blotting was performed as described above, using a monoclonal Flag-Tag antibody (1:2000, Pierce, Thermo Scientific).

NOTCH gene expression in white blood cells

White blood cells were isolated from peripheral blood using Lymphocyte Separation Medium (Lonza, Basel, Switzerland) from patients III.6 and IV.5, and from age matched healthy controls. Total RNA was extracted from primary cultured fibroblasts using RNeasy kit (Qiagen, Hilden, Germany) according to supplier's instructions. RNA was reverse transcribed and amplified by qPCR reaction as reported above. Primers were described in the **Supplementary table 2**.

rAAV vectors

Recombinant AAV vectors were prepared by the AAV Vector Unit at the International Centre for Genetic Engineering and Biotechnology Trieste as described previously[63]. In brief, infectious AAV6 vector particles were generated in HEK293 cells by cotransfecting each vector plasmid (pAAV-MIB2^{WT}, - MIB2^{V742G}, - MIB2^{V984L}, vector and pAAV-MCS) together with the packaging plasmid (pAAV6-2[64] and helper plasmid (pHELPER; Stratagene), expressing AAV and adenovirus helper functions, respectively. Viral stocks were obtained by $CsCl_2$ gradient centrifugation; rAAV titers, determined by measuring the copy number of viral genomes in pooled, dialyzed gradient fractions, as described previously [65], were in the range of $1x10^{10}$ to $1x10^{13}$ vg/ml.

Rat primary cardiomyocytes

Animal care and treatment were performed following the Institutional Guidelines in compliance to National and International laws and policies. Wistar rats were purchased from Charles River Laboratories Italia and maintained under controlled environmental conditions. Ventricular cardiomyocytes from neonatal rats were isolated as previously described[24]. In brief, ventricles from neonatal rats (post-natal day 1) were separated from the atria, cut into pieces and dissociated in CBFHH (calcium and bicarbonate-free Hanks with Hepes) buffer containing 2 mg/ml of trypsin (BD Difco) and 20 µg/ml of DNase II (Sigma) under constant stirring. Digestion was performed at room temperature in eight-to-ten 10-min steps, collecting the supernatant after each step. The supernatants were centrifuged to separate the cells which were then resuspended in

Dulbecco's modified Eagle medium 4.5 g/L glucose (DMEM, Life Technologies) supplemented with 5% FBS, 20 µg/ml vitamin B12 (Sigma), 100 U/ml penicillin and 100 µg/ml of streptomycin (Sigma). The collected cells were filtered through a cell strainer (40 µm, BD Falcon), and then seeded onto uncoated 100-mm plastic dishes for 2 hours at 37°C in 5% CO_2 and humidified atmosphere. The supernatant composed mostly of cardiomyocytes was then collected and plated. Cultures of neonatal rat ventricular cardiomyocytes prepared by this procedure yielded consistently a purity >90%. In the experiments with AAV-mediated gene transfer, neonatal rat cardiomyocytes were infected immediately after isolation using $1x10^5$ viral genomes (vg)/cell. Twelve hours later, the culture medium was changed and cells were subjected to the different treatments and subsequent analyses.

Functional studies in primary cardiomyocytes

To detect Notch1 activity under different experimental conditions, neonatal cardiomyocytes were seeded onto 96-well primary cells culture plates ($1.5\ x10^4$ cells per well) and transduced with AAV6-MIB2^{WT}, AAV6- MIB2^{V742G}, AAV6- MIB2^{V984L}, or an empty AAV6-MCS vector (moi=$1x10^5$ vg/cell). The day after the infection, cardiomyocytes were co-transfected with 0.5 µg of 4XCBF1-Luc reporter plasmid and 0.01 µg pRL-Renilla (which was used as an efficiency control) by using Lipofectamine 2000 transfection reagent (Invitrogen). After 6 hrs of incubation, medium was removed and cells were fed in complete medium for 8 hrs in DMSO (control) or GSI containing medium [DAPT (N-[N-(3,5-difluorophenacetyl)-L-alanyl]-S-phenylglycine t-butyl ester)-20µM] prior to lysis in PLB buffer (Promega). Firefly luciferase activity was corrected for the transfection efficiency by using the control Renilla luciferase activity in each sample. Firefly and Renilla luciferase activities were assayed with the Dual-luciferase assay kit (Promega).

Cardiomyocyte proliferation was analyzed 4 days after their isolation. Cells transduced with either AAV6-MIB2^{WT}, or AAV6- MIB2^{V742}G, or AAV6- MIB2^{V984L}, vector (moi=$1x10^5$ vg/cell) were grown in culture medium supplemented with 5 µM 5-ethynyl-2'-deoxyuridine (EdU, Life

Technologies) for 8 hrs. Cells were fixed with 4% paraformaldehyde for 10 min, permeabilized with 0.1% Triton X-100 in phosphate buffered saline (PBS) for 10 min, followed by 1 hr blocking in 2% BSA (Roche) in PBS. Cells were then stained over night at 4°C with the mouse anti α-sarcomeric actinin (EA-53), 1:100 (AbCam). Cells were washed with PBS and incubated for 1 hr with the secondary antibodies goat anti-mouse conjugated to Alexa Fluor 488. All washes were in PBS 0.2% Tween 20. Cells were further processed using the Click-IT EdU 555 Imaging kit to reveal EdU incorporation, according to the manufacturer's instructions, and stained with Hoechst 33342 (Life Technologies).

Image acquisition was performed using an ImageXpress Micro automated high-content screening fluorescence microscope at 10X magnification; a total of 16 images were acquired per wavelength, well and replicate, corresponding to approximately 2,500 cells analyzed per condition and replicate. Image analysis was performed using the Multi-Wavelenght Cell Scoring application module implemented in MetaXpress software (Molecular Devices). In all quantifications, cardiomyocytes were distinguished from other cells present in the primary cultures by their positivity for sarcomeric a-actinin. Images were acquired at room temperature with a DMLB upright fluorescence microscope (Leica) equipped with a charge-coupled device camera (CoolSNAP CF; Roper Scientific) using MetaView 4.6 quantitative analysis software (MDS Analytical Technologies). Within each experiment, instrument settings were kept constant.

ACKNOWLEDGEMENTS

We thank the patients for participation to the study. We thank John Belmont and Hamed Jafar-Nejad for fruitful discussions and for critical review of the manuscript. This work was supported by a grant from the Italian Association for Cancer Research (AIRC) to N.B.-P and by the Indiana University Health - Indiana University School of Medicine Strategic Research Initiative (T.C.L., P.C.S., K.G.S. and M.V.).

URLs:

Picard: http://picard.sourceforge.net

Bioscope software manual: https://tools.lifetechnologies.com/content/sfs/manuals/cms_082377.pdf

EVS: http://evs.gs.washington.edu/EVS/

ExAC: http://exac.broadinstitute.org

REFERENCES

1. Chong, J.X., Buckingham, K.J., Jhangiani, S.N., Boehm, C., Sobreira, N., Smith, J.D., Harrell, T.M., McMillin, M.J., Wiszniewski, W., Gambin, T., et al. (2015). The Genetic Basis of Mendelian Phenotypes: Discoveries, Challenges, and Opportunities. Am J Hum Genet 97, 199-215.
2. Strisciuglio, C., Corleto, V.D., Brunetti-Pierri, N., Piccolo, P., Sangermano, R., Rindi, G., Martini, M., D'Armiento, F.P., Staiano, A., and Miele, E. (2012). Autosomal dominant Menetrier-like disease. J Pediatr Gastroenterol Nutr 55, 717-720.
3. Coffey, R.J., Washington, M.K., Corless, C.L., and Heinrich, M.C. (2007). Menetrier disease and gastrointestinal stromal tumors: hyperproliferative disorders of the stomach. J Clin Invest 117, 70-80.
4. Larsen, B., Tarp, U., and Kristensen, E. (1987). Familial giant hypertrophic gastritis (Menetrier's disease). Gut 28, 1517-1521.
5. Bockman, D.E., Sharp, R., and Merlino, G. (1995). Regulation of terminal differentiation of zymogenic cells by transforming growth factor alpha in transgenic mice. Gastroenterology 108, 447-454.
6. Sharp, R., Babyatsky, M.W., Takagi, H., Tagerud, S., Wang, T.C., Bockman, D.E., Brand, S.J., and Merlino, G. (1995). Transforming growth factor alpha disrupts the normal program of cellular differentiation in the gastric mucosa of transgenic mice. Development 121, 149-161.
7. Takeda, T., Mitsuyama, K., Tsuruta, O., Kuboyama, S., Kitazaki, S., and Sata, M. (2006). Role of vascular endothelial growth factor in protein loss of Menetrier's disease. Int J Mol Med 18, 571-576.
8. Noguchi, T.K., Ninomiya, N., Sekine, M., Komazaki, S., Wang, P.C., Asashima, M., and Kurisaki, A. (2015). Generation of stomach tissue from mouse embryonic stem cells. Nat Cell Biol 17, 984-993.
9. Fiske, W.H., Tanksley, J., Nam, K.T., Goldenring, J.R., Slebos, R.J., Liebler, D.C., Abtahi, A.M., La Fleur, B., Ayers, G.D., Lind, C.D., et al. (2009). Efficacy of cetuximab in the treatment of Menetrier's disease. Sci Transl Med 1, 8ra18.
10. Lam, S.K., Hui, W.K., Ho, J., Wong, K.P., Rotter, J.I., and Samloff, I.M. (1983). Pachydermoperiostosis, hypertrophic gastropathy, and peptic ulcer. Gastroenterology 84, 834-839.

11. Marcus, P., and Verp, M.S. (1993). Menetrier disease in a child of a consanguineous union. Am J Med Genet 47, 1231-1232.
12. Mosavi, L.K., Minor, D.L., Jr., and Peng, Z.Y. (2002). Consensus-derived structural determinants of the ankyrin repeat motif. Proceedings of the National Academy of Sciences of the United States of America 99, 16029-16034.
13. Tang, K.S., Fersht, A.R., and Itzhaki, L.S. (2003). Sequential unfolding of ankyrin repeats in tumor suppressor p16. Structure 11, 67-73.
14. Kamburov, A., Lawrence, M.S., Polak, P., Leshchiner, I., Lage, K., Golub, T.R., Lander, E.S., and Getz, G. (2015). Comprehensive assessment of cancer missense mutation clustering in protein structures. Proceedings of the National Academy of Sciences of the United States of America 112, E5486-5495.
15. Vazquez, M., Valencia, A., and Pons, T. (2015). Structure-PPi: a module for the annotation of cancer-related single-nucleotide variants at protein-protein interfaces. Bioinformatics 31, 2397-2399.
16. Cheng, C., Lingyan, W., Yi, H., Cheng, Z., Huadan, Y., Xuting, X., Leiting, X., Meng, Y., and Shiwei, D. (2014). Association between TLR2, MTR, MTRR, XPC, TP73, TP53 genetic polymorphisms and gastric cancer: a meta-analysis. Clin Res Hepatol Gastroenterol 38, 346-359.
17. Findlay, J.M., Middleton, M.R., and Tomlinson, I. (2015). A systematic review and meta-analysis of somatic and germline DNA sequence biomarkers of esophageal cancer survival, therapy response and stage. Ann Oncol 26, 624-644.
18. Luxan, G., Casanova, J.C., Martinez-Poveda, B., Prados, B., D'Amato, G., MacGrogan, D., Gonzalez-Rajal, A., Dobarro, D., Torroja, C., Martinez, F., et al. (2013). Mutations in the NOTCH pathway regulator MIB1 cause left ventricular noncompaction cardiomyopathy. Nature medicine 19, 193-201.
19. Fang, S., Jensen, J.P., Ludwig, R.L., Vousden, K.H., and Weissman, A.M. (2000). Mdm2 is a RING finger-dependent ubiquitin protein ligase for itself and p53. The Journal of biological chemistry 275, 8945-8951.
20. Takeuchi, T., Adachi, Y., and Ohtsuki, Y. (2005). Skeletrophin, a novel ubiquitin ligase to the intracellular region of Jagged-2, is aberrantly expressed in multiple myeloma. The American journal of pathology 166, 1817-1826.
21. Koo, B.K., Yoon, K.J., Yoo, K.W., Lim, H.S., Song, R., So, J.H., Kim, C.H., and Kong, Y.Y. (2005). Mind bomb-2 is an E3 ligase for Notch ligand. The Journal of biological chemistry 280, 22335-22342.
22. Hsieh, J.J., Henkel, T., Salmon, P., Robey, E., Peterson, M.G., and Hayward, S.D. (1996). Truncated mammalian Notch1 activates CBF1/RBPJk-repressed genes by a mechanism resembling that of Epstein-Barr virus EBNA2. Mol Cell Biol 16, 952-959.
23. Lovric, J., Mano, M., Zentilin, L., Eulalio, A., Zacchigna, S., and Giacca, M. (2012). Terminal differentiation of cardiac and skeletal myocytes induces permissivity to AAV transduction by relieving inhibition imposed by DNA damage response proteins. Mol Ther 20, 2087-2097.
24. Collesi, C., Zentilin, L., Sinagra, G., and Giacca, M. (2008). Notch1 signaling stimulates proliferation of immature cardiomyocytes. J Cell Biol 183, 117-128.
25. Occena, R.O., Taylor, S.F., Robinson, C.C., and Sokol, R.J. (1993). Association of cytomegalovirus with Menetrier's disease in childhood: report of two new cases with a review of literature. J Pediatr Gastroenterol Nutr 17, 217-224.
26. Li, X.J., Liu, X.J., Yang, B., Fu, Y.R., Zhao, F., Shen, Z.Z., Miao, L.F., Rayner, S., Chavanas, S., Zhu, H., et al. (2015). Human Cytomegalovirus Infection Dysregulates the Localization and Stability of NICD1 and Jag1 in Neural Progenitor Cells. J Virol 89, 6792-6804.
27. Zhang, X., Yang, Y., Zhu, R., Bai, J., Tian, Y., Li, X., Peng, Z., He, Y., Chen, L., Fang, D., et al. (2012). H. pylori induces the expression of Hath1 in gastric epithelial cells via

interleukin-8/STAT3 phosphorylation while suppressing Hes1. J Cell Biochem 113, 3740-3751.
28. Perez-Ramirez, M., Hernandez-Jimenez, A.J., Guerrero-Guerrero, A., Benadon-Darszon, E., Perezpena-Diazconti, M., Siordia-Reyes, A.G., Garcia-Mendez, A., de Leon, F.C., Salamanca-Gomez, F.A., and Garcia-Hernandez, N. (2016). Genomics and epigenetics: A study of ependymomas in pediatric patients. Clin Neurol Neurosurg 144, 53-58.
29. Wang, C., Guo, X., and Xi, R. (2014). EGFR and Notch signaling respectively regulate proliferative activity and multiple cell lineage differentiation of Drosophila gastric stem cells. Cell research 24, 610-627.
30. Kim, T.H., and Shivdasani, R.A. (2011). Notch signaling in stomach epithelial stem cell homeostasis. The Journal of experimental medicine 208, 677-688.
31. Aguirre, A., Rubio, M.E., and Gallo, V. (2010). Notch and EGFR pathway interaction regulates neural stem cell number and self-renewal. Nature 467, 323-327.
32. Bainbridge, M.N., Davis, E.E., Choi, W.Y., Dickson, A., Martinez, H.R., Wang, M., Dinh, H., Muzny, D.M., Pignatelli, R., Katsanis, N., et al. (2015). Loss of Function Mutations in NNT Are Associated With Left Ventricular Noncompaction. Circ Cardiovasc Genet 8, 544-552.
33. Xing, Y., Ichida, F., Matsuoka, T., Isobe, T., Ikemoto, Y., Higaki, T., Tsuji, T., Haneda, N., Kuwabara, A., Chen, R., et al. (2006). Genetic analysis in patients with left ventricular noncompaction and evidence for genetic heterogeneity. Mol Genet Metab 88, 71-77.
34. Klaassen, S., Probst, S., Oechslin, E., Gerull, B., Krings, G., Schuler, P., Greutmann, M., Hurlimann, D., Yegitbasi, M., Pons, L., et al. (2008). Mutations in sarcomere protein genes in left ventricular noncompaction. Circulation 117, 2893-2901.
35. Towbin, J.A., Lorts, A., and Jefferies, J.L. (2015). Left ventricular non-compaction cardiomyopathy. Lancet.
36. D'Amato, G., Luxan, G., Del Monte-Nieto, G., Martinez-Poveda, B., Torroja, C., Walter, W., Bochter, M.S., Benedito, R., Cole, S., Martinez, F., et al. (2016). Sequential Notch activation regulates ventricular chamber development. Nat Cell Biol 18, 7-20.
37. Luxan, G., D'Amato, G., MacGrogan, D., and de la Pompa, J.L. (2016). Endocardial Notch Signaling in Cardiac Development and Disease. Circ Res 118, e1-e18.
38. Grego-Bessa, J., Luna-Zurita, L., del Monte, G., Bolos, V., Melgar, P., Arandilla, A., Garratt, A.N., Zang, H., Mukouyama, Y.S., Chen, H., et al. (2007). Notch signaling is essential for ventricular chamber development. Developmental cell 12, 415-429.
39. Sen-Chowdhry, S., and McKenna, W.J. (2008). Left ventricular noncompaction and cardiomyopathy: cause, contributor, or epiphenomenon? Curr Opin Cardiol 23, 171-175.
40. Shou, W., Aghdasi, B., Armstrong, D.L., Guo, Q., Bao, S., Charng, M.J., Mathews, L.M., Schneider, M.D., Hamilton, S.L., and Matzuk, M.M. (1998). Cardiac defects and altered ryanodine receptor function in mice lacking FKBP12. Nature 391, 489-492.
41. Petersen, S.E., Selvanayagam, J.B., Wiesmann, F., Robson, M.D., Francis, J.M., Anderson, R.H., Watkins, H., and Neubauer, S. (2005). Left ventricular non-compaction: insights from cardiovascular magnetic resonance imaging. J Am Coll Cardiol 46, 101-105.
42. Gati, S., Merghani, A., and Sharma, S. (2015). Increased left ventricular trabeculation does not necessarily equate to left ventricular noncompaction in athletes. JAMA Intern Med 175, 461-462.
43. Mutarelli, M., Marwah, V., Rispoli, R., Carrella, D., Dharmalingam, G., Oliva, G., and di Bernardo, D. (2014). A community-based resource for automatic exome variant-calling and annotation in Mendelian disorders. BMC genomics 15 Suppl 3, S5.
44. Li, H., and Durbin, R. (2009). Fast and accurate short read alignment with Burrows-Wheeler transform. Bioinformatics 25, 1754-1760.
45. Li, H., Handsaker, B., Wysoker, A., Fennell, T., Ruan, J., Homer, N., Marth, G., Abecasis, G., Durbin, R., and Genome Project Data Processing, S. (2009). The Sequence Alignment/Map format and SAMtools. Bioinformatics 25, 2078-2079.

46. DePristo, M.A., Banks, E., Poplin, R., Garimella, K.V., Maguire, J.R., Hartl, C., Philippakis, A.A., del Angel, G., Rivas, M.A., Hanna, M., et al. (2011). A framework for variation discovery and genotyping using next-generation DNA sequencing data. Nature genetics 43, 491-498.
47. Wang, K., Li, M., and Hakonarson, H. (2010). ANNOVAR: functional annotation of genetic variants from high-throughput sequencing data. Nucleic acids research 38, e164.
48. Pruitt, K.D., Tatusova, T., Brown, G.R., and Maglott, D.R. (2012). NCBI Reference Sequences (RefSeq): current status, new features and genome annotation policy. Nucleic acids research 40, D130-135.
49. Sherry, S.T., Ward, M.H., Kholodov, M., Baker, J., Phan, L., Smigielski, E.M., and Sirotkin, K. (2001). dbSNP: the NCBI database of genetic variation. Nucleic acids research 29, 308-311.
50. Hamosh, A., Scott, A.F., Amberger, J.S., Bocchini, C.A., and McKusick, V.A. (2005). Online Mendelian Inheritance in Man (OMIM), a knowledgebase of human genes and genetic disorders. Nucleic acids research 33, D514-517.
51. Stenson, P.D., Mort, M., Ball, E.V., Shaw, K., Phillips, A., and Cooper, D.N. (2014). The Human Gene Mutation Database: building a comprehensive mutation repository for clinical and molecular genetics, diagnostic testing and personalized genomic medicine. Human genetics 133, 1-9.
52. Landrum, M.J., Lee, J.M., Riley, G.R., Jang, W., Rubinstein, W.S., Church, D.M., and Maglott, D.R. (2014). ClinVar: public archive of relationships among sequence variation and human phenotype. Nucleic acids research 42, D980-985.
53. Genomes Project, C., Abecasis, G.R., Altshuler, D., Auton, A., Brooks, L.D., Durbin, R.M., Gibbs, R.A., Hurles, M.E., and McVean, G.A. (2010). A map of human genome variation from population-scale sequencing. Nature 467, 1061-1073.
54. Pollard, K.S., Hubisz, M.J., Rosenbloom, K.R., and Siepel, A. (2010). Detection of nonneutral substitution rates on mammalian phylogenies. Genome research 20, 110-121.
55. Goode, D.L., Cooper, G.M., Schmutz, J., Dickson, M., Gonzales, E., Tsai, M., Karra, K., Davydov, E., Batzoglou, S., Myers, R.M., et al. (2010). Evolutionary constraint facilitates interpretation of genetic variation in resequenced human genomes. Genome research 20, 301-310.
56. Kumar, P., Henikoff, S., and Ng, P.C. (2009). Predicting the effects of coding non-synonymous variants on protein function using the SIFT algorithm. Nature protocols 4, 1073-1081.
57. Adzhubei, I., Jordan, D.M., and Sunyaev, S.R. (2013). Predicting functional effect of human missense mutations using PolyPhen-2. Current protocols in human genetics / editorial board, Jonathan L Haines [et al] Chapter 7, Unit7 20.
58. Liu, X., Jian, X., and Boerwinkle, E. (2011). dbNSFP: a lightweight database of human nonsynonymous SNPs and their functional predictions. Human mutation 32, 894-899.
59. Schwarz, J.M., Rodelsperger, C., Schuelke, M., and Seelow, D. (2010). MutationTaster evaluates disease-causing potential of sequence alterations. Nature methods 7, 575-576.
60. Kircher, M., Witten, D.M., Jain, P., O'Roak, B.J., Cooper, G.M., and Shendure, J. (2014). A general framework for estimating the relative pathogenicity of human genetic variants. Nature genetics 46, 310-315.
61. Thorvaldsdottir, H., Robinson, J.T., and Mesirov, J.P. (2013). Integrative Genomics Viewer (IGV): high-performance genomics data visualization and exploration. Briefings in bioinformatics 14, 178-192.
62. Liu, X., Jian, X., and Boerwinkle, E. (2013). dbNSFP v2.0: a database of human non-synonymous SNVs and their functional predictions and annotations. Hum Mutat 34, E2393-2402.
63. Arsic, N., Zacchigna, S., Zentilin, L., Ramirez-Correa, G., Pattarini, L., Salvi, A., Sinagra, G., and Giacca, M. (2004). Vascular endothelial growth factor stimulates skeletal muscle regeneration in vivo. Mol Ther 10, 844-854.

64. Gao, G.P., Alvira, M.R., Wang, L., Calcedo, R., Johnston, J., and Wilson, J.M. (2002). Novel adeno-associated viruses from rhesus monkeys as vectors for human gene therapy. Proc Natl Acad Sci U S A 99, 11854-11859.
65. Zentilin, L., Marcello, A., and Giacca, M. (2001). Involvement of cellular double-strand DNA break-binding proteins in processing of recombinant adeno-associated virus (AAV) genome. J Virol 75, 12279-12287.

FIGURE LEGENDS

Figure 1. (**A**) Pedigree of the family with inherited gastropathy and/or LVNC. (**C**) EGFR staining in gastric specimens from two affected individuals from pedigree and a control (Ctrl). (**D**) Cardiac ultrasound and MRI of patients with LVNC from the one subject of the pedigree harboring the p.V742G variants (subject IV.2) and the isolated case with the p.V984L variant.

Figure 2. (A and **B)** Mapping of *MIB2* mutations onto the 3D models of Ankyrin-repeat and Zinc finger C3HC4 or RING-type motif. (**C** and **D**) Western blotting with antibody against the ubiquitinated FLAG after incubation of purified wild-type and mutated MIB2 proteins with E1, E2 proteins, and FLAG-Ubiquitin. The quantitation of the intensities of protein bands corresponding to ubiquitinated FLAG normalized for MIB2 protein band are shown in D. (**E**) Decreased stability of $MIB2^{V984L}$ mutant in transfected primary rat cardiomyocytes. Relative quantification of the amounts of $MIB2^{WT}$, $MIB2^{V742G}$ and $MIB2^{V984L}$ proteins in HEK293 cells incubated with cycloheximide (CHX). In the graph, the amount of MIB2 was set at 100% in samples maintained 4 hours in the presence of 10 μM proteasome inhibitor MG132. Results are expressed as average ± SD of three separate experiments. *$p<0.05$.

Figure 3. Expression of NOTCH signaling genes in blood lymphocytes of two affected members from the pedigree (III.6 and IV.5) compared to age- and gender-matched controls. Average ± SEM are shown.

Figure 4. (A) Notch signaling activity measured by 4XCBF1-Luc reporter assay. Primary rat cardiomyocytes were transfected with 4XCBF1 firefly luciferase reporter and renilla-luciferase reporter for normalization. DAPT treatment reduced 4XCBF1-luciferase reporter activation and was used as a specific transactivation control. (**B**) An ATP-Lite assay and proliferation assay (**C-D**) on freshly isolated rat neonatal cardiomyocytes transduced with AAV6 vectors encoding $MIB2^{WT}$,

MIB2^{V742G}, or MIB2^{V984L} (m.o.i. = 1x10^5 vg/cell). Representative images of at least 5 separate experiments of EdU$^+$ cardiomyocytes after AAV-mediated gene transfer are shown in **C**. Green, α-actinin; red, EdU; blue, DNA (DAPI). (**D**) Quantification of the total number of α-actinin+/EdU+ cells (proliferating cardiomyocytes) after 4 days of culture. Results are representative of at least three independent experiments. Mean±SD is shown. *, $p<0.05$; **, $p<0.01$.

Table 1. Variants detected by exome sequencing

Gene	Refseq	Variation	Frequency (ExAC)
NUP98	NM_016320	c.4573G>A (p.A1525T)	Not reported
MIB2	NM_080875	c.2225T>G (p.V742G)	0.0015 (172/116,536 alleles)
SLC10A2	NM_000452	c.475G>A (p.V159I)	0.01795 (2,178/121,346 alleles)
SIDT1	NM_017699	c.232G>A (p.V78M)	0.04059 (4,920/121,220 alleles)
SPICE1	NM_144718	c.823C>G (p.L275V)	0.04793 (5,799/120,984 alleles)
ZNF781	NM_152605	c.290C>T (p.T97M)	0.05046 (6,125/121,374 alleles)
KCNJ12	NM_001194958	c.517G>A (p.D173N)	0.4731 (53,101/112,234 alleles)
GPRIN2	NM_014696	c.298A>C (p.T100P)	0.4838 (57,014/117,836 alleles)

Table 2. Frequency of *MIB2* variants in human genome variant databases

Database	**Frequency**		
	c.214T>C (p.F72L) **rs7418389**	**c.2225T>G (p.V742G)** **rs7418389**	**c.2950G>C (p.V984L)**
ExAC	0.6228 (61,204/98,272 alleles)	0.0015 (172/116,536 alleles)	$9.8x10^{-6}$ (1/102,118 alleles)
EVS	0,6709 (8,086/12,056 alleles)	Not reported	Not reported
1000genomes	0.477 (2,389/5,008 alleles)	0.003 (14/ 4,994 alleles)	Not reported

SUPPLEMENTARY ONLINE MATERIAL

Supplementary Table 1. *In silico* predictions of pathogenicity of *MIB2* mutations.

		c.2225T>G (p.V742G)		**c.2950G>C (p.V984L)**	
Classification	**Method**	**Score**	**Prediction**	**Score**	**Prediction**
Sequence-based methods	Polyphen-2	0.998	probably damaging	0.005	Neutral
	SIFT	0.02	damaging	0.42	Neutral
	Mutation-Assessor	3.655	functional Impact high	0.585	Neutral
	SVM	0.22	Deleterious	-0.979	Neutral
	VEST3	0.89	Deleterious	0.174	Neutral
Structure-based methods		**ΔΔG (kcal/mol)**		**ΔΔG (kcal/mol)**	
	I-Mutant 2.0	-2.69	Decrease 3D stability	-0.7	Decrease 3D stability
	PoPMuSiC	2.57	Decrease 3D stability	0.49	Decrease 3D stability
	CUPSAT	-8.30	Decrease 3D stability	0.86	Increase 3D stability

Supplementary table 2. Real-time PCR primers

Primer name	**Sequence**
DTX-for	5’-ACGAGAAAGGCCGGAAGGT-3’

DTX-rev	5’-GGTGTTGGACGTGCCGATAG-3’
HES1-for	5’-CCTGTCATCCCCGTCTACAC-3’
HES1-rev	5’-CACATGGAGTCCGCCGTAA-3’
NOTCH3-for	5’-CGTGGCTTCTTTCTACTGTGC-3’
NOTCH3-rev	5’-CGTTCACCGGATTTGTGTCAC-3’
NRARP-for	5’-TCAACGTGAACTCGTTCGGG-3’
NRARP-rev	5’-ACTTCGCCTTGGTGATGAGAT-3’
HEY-for	5’-GTTCGGCTCTAGGTTCCATGT-3’
HEY-rev	5’-CGTCGGCGCTTCTCAATTATTC-3’
GUSB-for	5’-CAACGAGCCTGCGTCCCACC-3’
GUSB-rev	5’-ACGGAGCCCCCTTGTCTGCT-3’
HPRT1-for	5’-TGGCGTCGTGATTAGTGATG-3’
HPRT1-rev	5’-AACACCCTTTCCAAATCCTCAG-3’

Supplementary Figure 1. Segregation of the p.P33R polymorphism in *TP53* gene in family with LNVC and inherited gastropathy.

Supplementary Figure 2. Electrocardiogram (EKG) of the non-familiar case with LVNC showing sinus rhythm with premature supraventricular complexes, nonspecific T wave abnormality with a QTc interval of 450 ms.

Supplementary Figure 3. (**A**) Western blotting with two different antibodies recognizing different epitopes in protein extracts of HeLa cells co-transfected with plasmids expressing the wild-type or mutant MIB2 proteins and a plasmid expressing GFP, as an internal control of transfection

efficiency. (**B**) Real time PCR levels of MIB2 in HeLa cells co-transfected with plasmids expressing the wild-type or mutant MIB2 proteins.

Supplementary Figure 4. Expression levels of $MIB2^{WT}$, $MIB2^{V742G}$, or $MIB2^{V984L}$ in cardiomyocytes transduced with AAV6.

FIG. 1

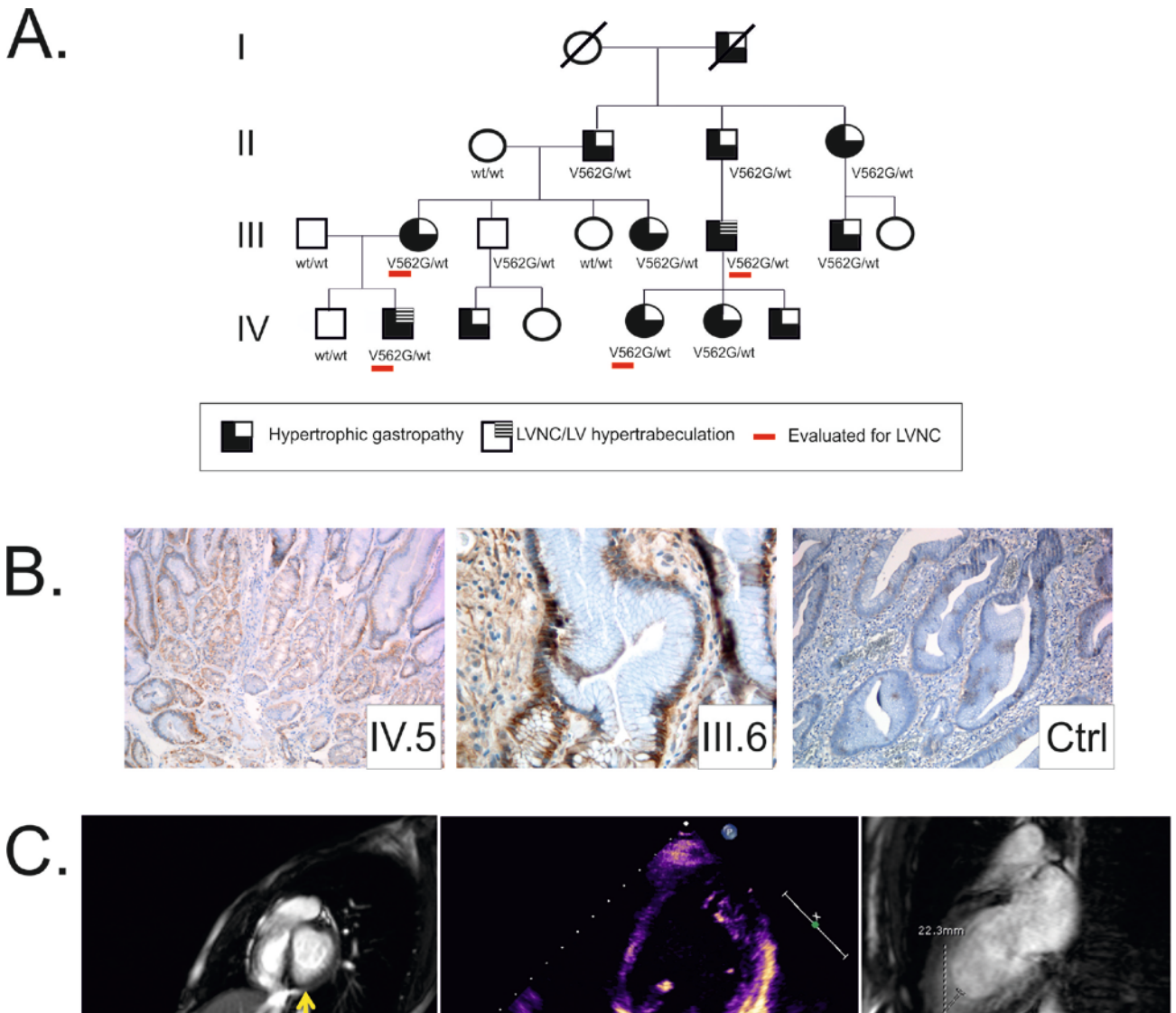
A.
I
II
III
IV
wt/wt
V562G/wt
Hypertrophic gastropathy
LVNC/LV hypertrabeculation
Evaluated for LVNC
B.
IV.5
III.6
Ctrl
C.
LV
22.3mm
8.76mm
MIB2V742G
MIB2V984L

FIG. 2

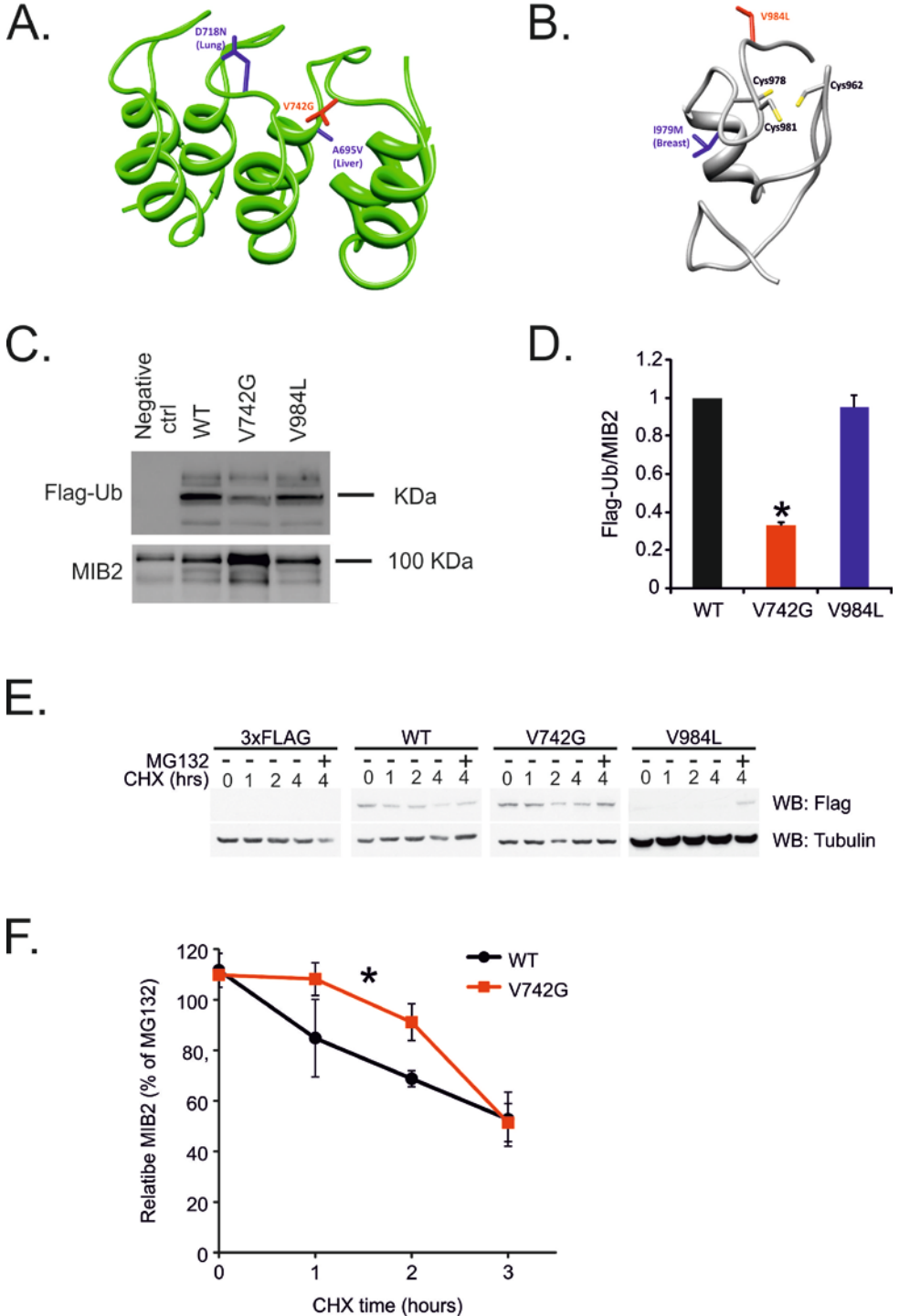
A.
D718N
(Lung)
V742G
A695V
(Liver)
B.
V984L
Cys978
Cys962
Cys981
I979M
(Breast)
C.
Negative ctrl
WT
V742G
V984L
Flag-Ub
KDa
MIB2
100 KDa
D.
Flag-Ub/MIB2
1.2
1
0.8
0.6
0.4
0.2
0
*
WT
V742G
V984L
E.
3xFLAG
WT
V742G
V984L
MG132
CHX (hrs)
0 1 2 4 4
WB: Flag
WB: Tubulin
F.
Relatibe MIB2 (% of MG132)
120
100
80,
60
40
20
0
*
WT
V742G
0
1
2
3
CHX time (hours)

FIG. 3

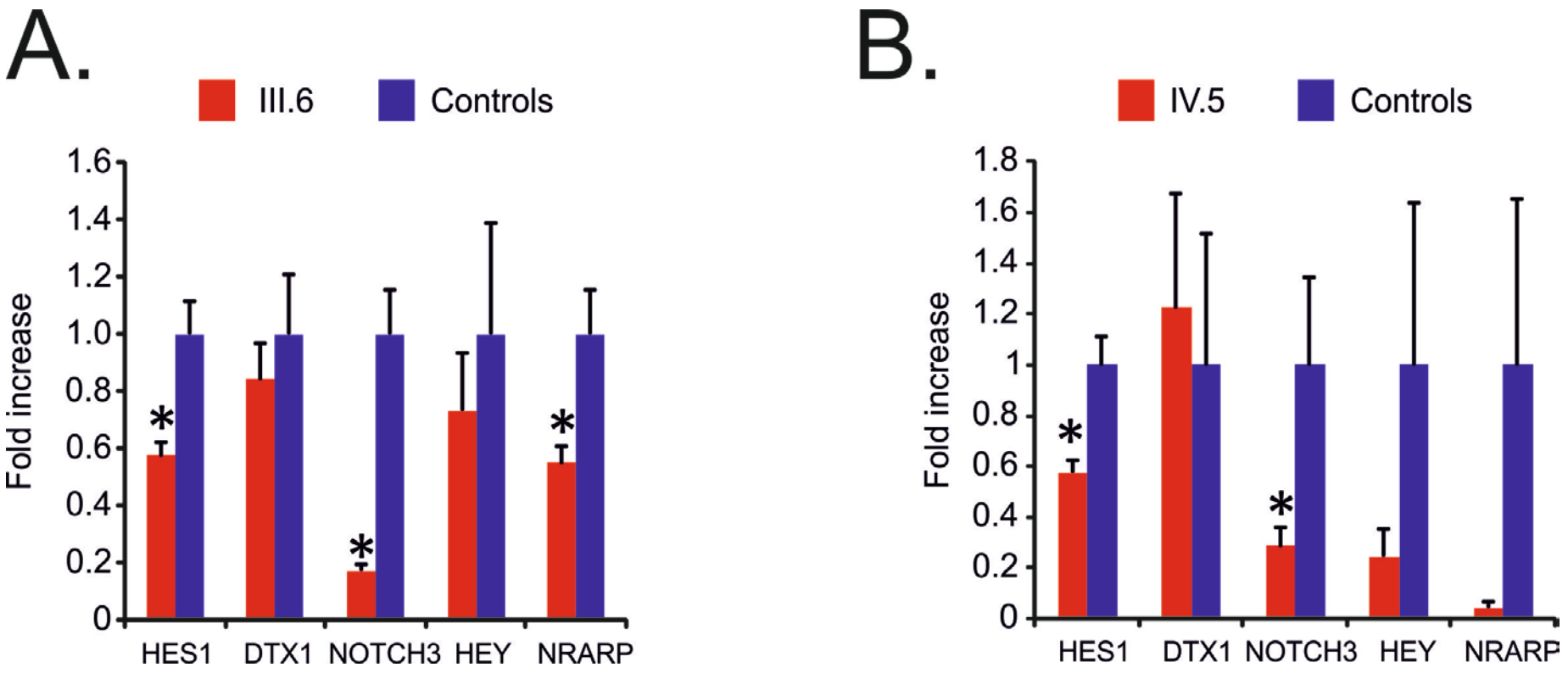
A.
III.6
Controls
Fold increase
1.6
1.4
1.2
1.0
0.8
0.6
0.4
0.2
0
HES1
DTX1
NOTCH3
HEY
NRARP
B.
IV.5
Controls
Fold increase
1.8
1.6
1.4
1.2
1
0.8
0.6
0.4
0.2
0
HES1
DTX1
NOTCH3
HEY
NRARP

FIG. 4

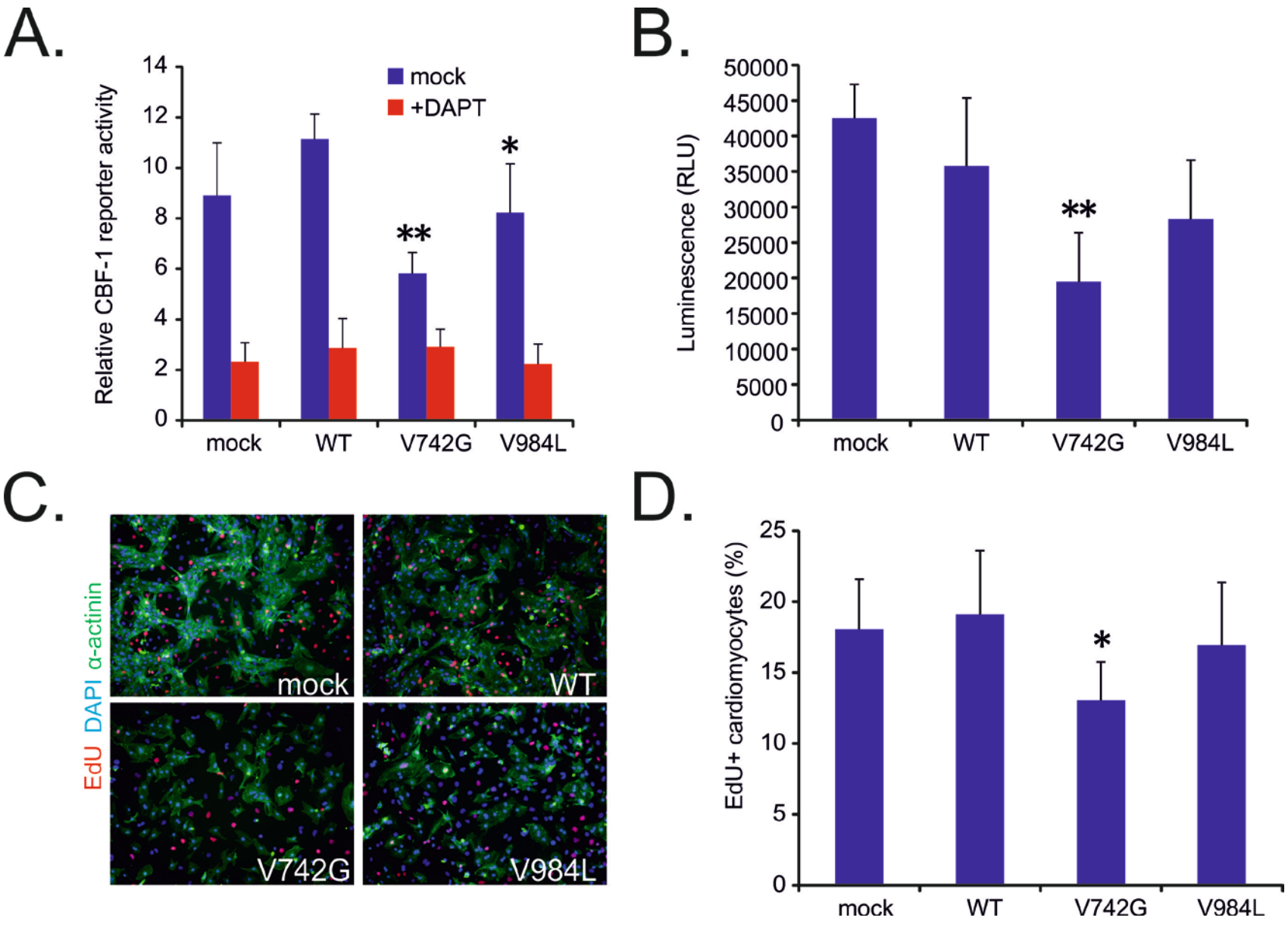
A.
Relative CBF-1 reporter activity
14
12
10
8
6
4
2
0
mock
+DAPT
**
*
mock
WT
V742G
V984L
B.
Luminescence (RLU)
50000
45000
40000
35000
30000
25000
20000
15000
10000
5000
0
**
mock
WT
V742G
V984L
C.
EdU DAPI α-actinin
mock
WT
V742G
V984L
D.
EdU+ cardiomyocytes (%)
25
20
15
10
5
0
*
mock
WT
V742G
V984L

Supplementary FIG. 1

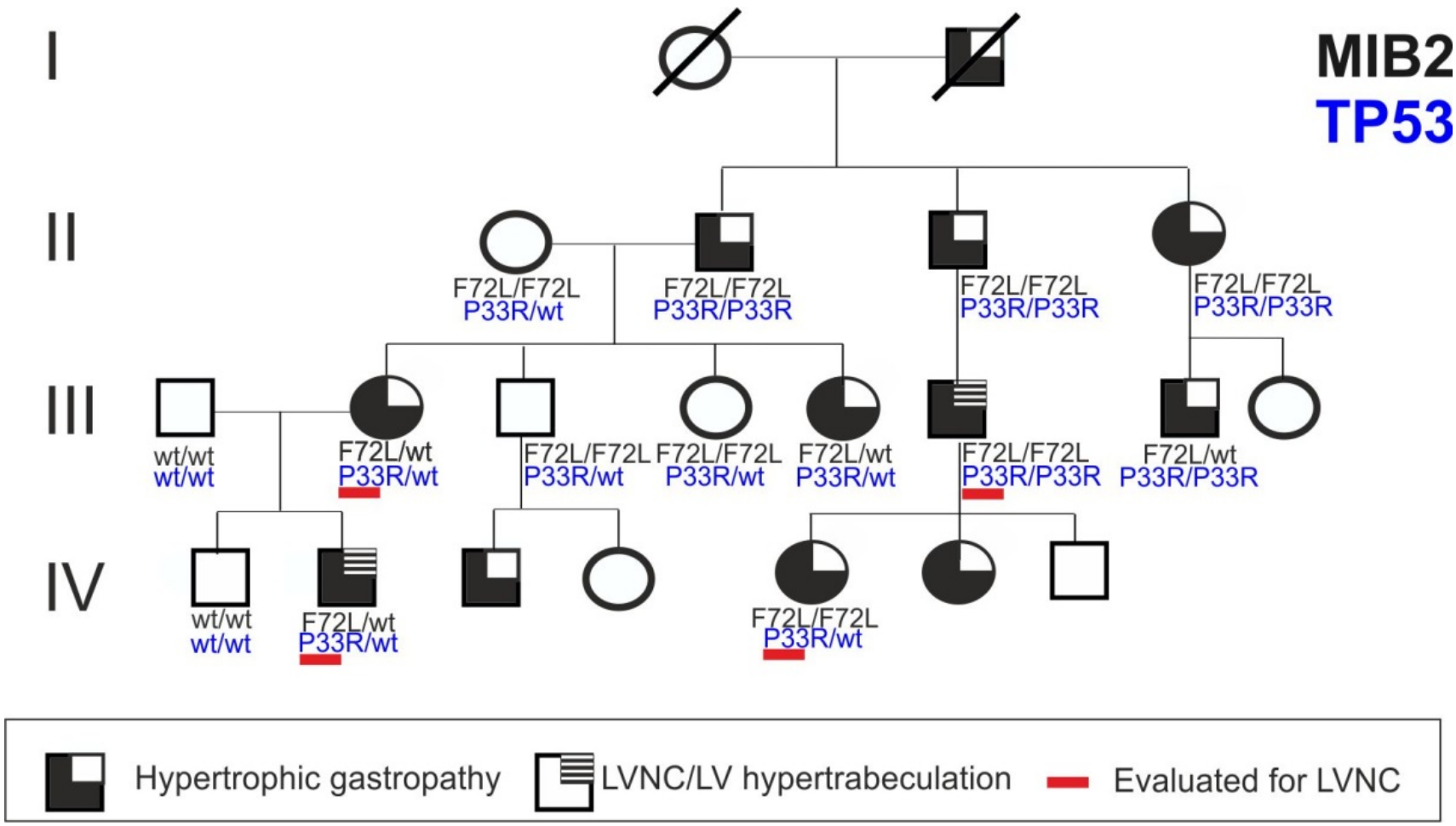

Supplementary FIG. 2

Vent. rate	74	BPM	Sinus rhythm with Premature supraventricular complexes
PR interval	130	ms	Nonspecific T wave abnormality
QRS duration	82	ms	Abnormal ECG
QT/QTc	406/450	ms	When compared with ECG of 16-JAN-2014 08:36,
P-R-T axes	90 83	68	Premature supraventricular complexes are now Present
BP	162/68		Confirmed by KOVACS , M.D., RICHARD (116) on 12/19/2014 9:59:48 AM

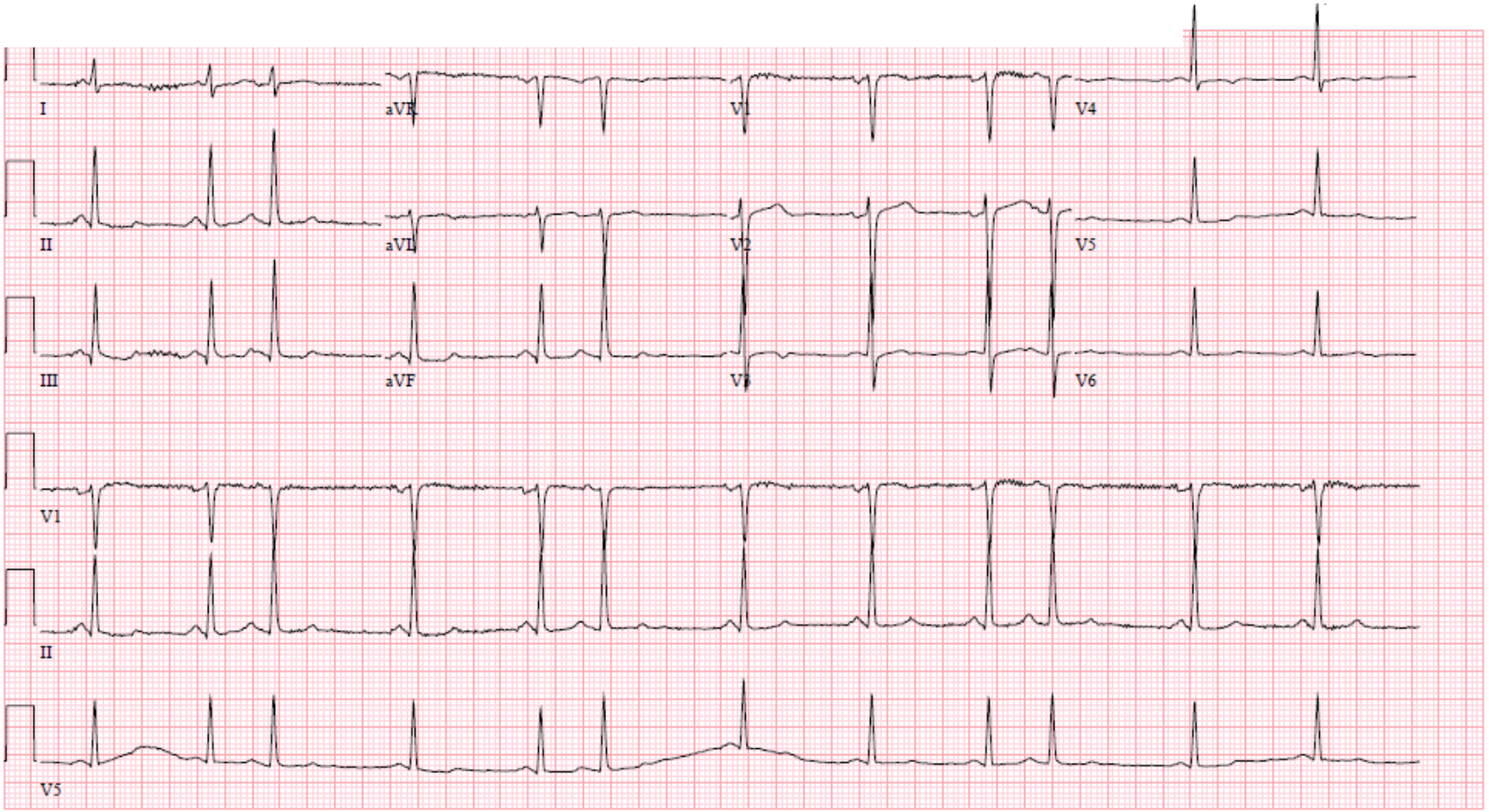

Supplementary FIG. 3

A.

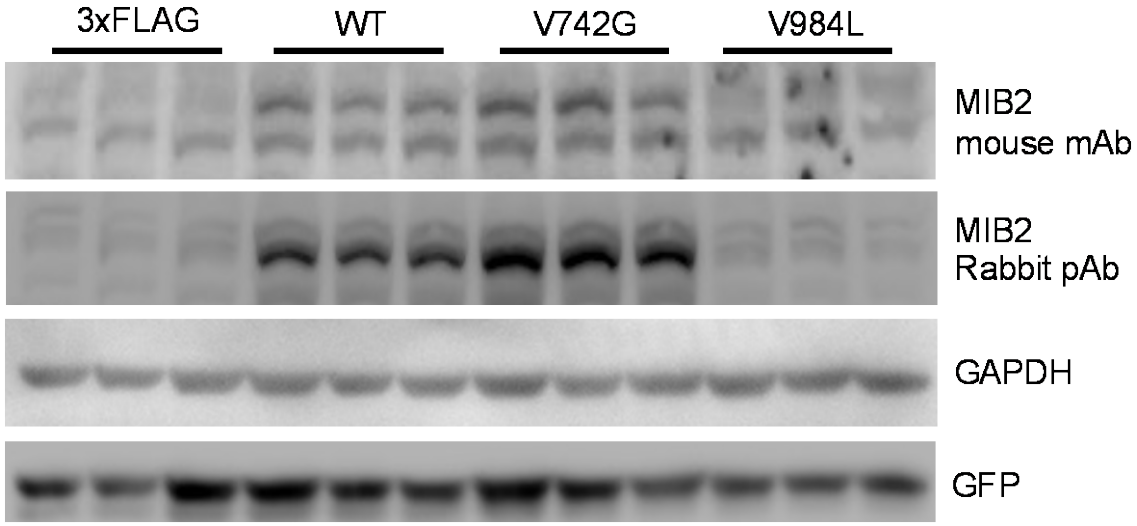

B.

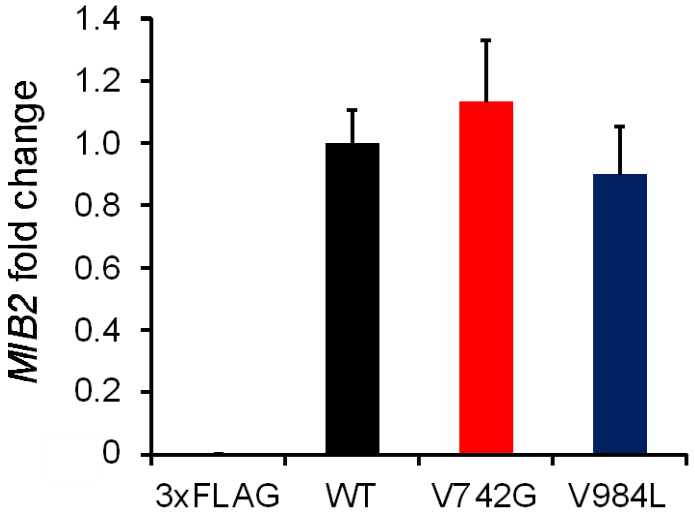

Supplementary FIG. 4